JET-P(95)19

The Plasma Shape and Current Control System of JET

M Garribba, R Litunovsky, S Puppin.

JET Joint Undertaking, Abingdon, Oxfordshire, OX14 3EA, UK.

Preprint of a paper to be submitted for publication in
Fusion Technology

June 1995

1. Introduction

The paper summarises the design and the experimental results obtained with the new Plasma Shape and Current Control system (SC) of JET. This control system was brought in operation at the start of the 1994 plasma operation for the *Pumped Divertor phase* of the experiment.

It has demonstrated the feasibility of plasma-wall gap control in a reactor relevant tokamak together with the possibility of using on-line a fast full plasma boundary measurement technique based on a large number of magnetic signals.

Multiple Input Multiple Output (MIMO) design techniques have been used for the derivation of a suitable control structure. A multivariable decoupling controller capable of handling a combination of directly controlled circuit currents and plasma-wall gaps corresponding to the available number of degrees of freedom is the result of the work. During the pulse time evolution each circuit can be controlled in different ways. The control mode more appropriate for each phase of the pulse is chosen by the operator.

The flexible design of the controller allows to include up to six plasma-wall distances to be controlled simultaneously. The control matrix used are calculated in real time according to the selected feedback array.

2. Open Loop Model

The first step for deriving a suitable control law is to define an open loop model of the plant simple enough to be handled and capable of describing the model characteristics necessary to design the

control law. Various approaches can be taken and are described in the literature []. Here the simplest method, which consists of linearising the system equations around a given *plasma equilibrium position,* is used. This approach is sometimes described as a *perturbation model of the plasma equilibrium.* The technique applied is nothing else than the usual linearisation procedure used in the control textbooks for dealing with non linear systems.

The starting point for the model derivation are the following two non linear equations:

$$\mathbf{X} = \mathbf{X}\left(\mathbf{I}, \beta_p, l_i, \psi_{iron}\right) \qquad (1)$$

$$\frac{d}{dt}\left(\mathbf{M}\left(\psi_{iron}, \mathbf{X}, \beta_p, l_i\right)\mathbf{I}\right) + \mathbf{R}\,\mathbf{I} = \mathbf{V} \qquad (2)$$

where **I** is the array of N_C + 1 poloidal field currents including the plasma current, **V** is the array of N_C applied voltages, **X** is an array containing N_G plasma-wall distances (gaps). **M** is the matrix of mutual inductances describing the mutual interaction of the poloidal field coils and the plasma.

Equation (1) expresses the plasma force balance by means of the array of the chosen plasma shape parameters as functions of the Poloidal Field (PF) equilibrium currents, the iron core magnetisation status ψ_C, the plasma current profile, parametrised by the internal inductance l_i and the poloidal beta β_p. Written in explicit terms equation (1) is the Grad-Shafranov equation. The explicit form and the solution of the equation is of no interest for the modelling purposes. It is important to characterise the response of the plasma boundary to changes in the PF circuit currents.

The choice of the functional dependencies in (1) is quite arbitrary. Different choices of variables produce different models. The one selected in this paper highlights the dependency of the plasma shape from *controllable* quantities like the circuit currents **I** and *uncontrollable* ones like the plasma current profile and the iron core saturation level, or the vessel eddy currents. The model should be able to show the system dynamics and allow to determine a class of disturbances representing the plasma behaviour to quantify the system capability to reject them.

Since the desired response times are greater than the modes associated with the vessel eddy currents the effects of passive structures on the plasma shape are omitted in the model. Experimentally it will be seen that this choice is quite justified.

Another advantage is represented by the fact that the positive eigenvalue due to the vertical instability mode is not introduced in the model. In JET, the vertical instability time constants are about 3-5ms. The system can be regarded as being decoupled from vertical movements on that time scale. It is possible to analyse and close the vertical stabilisation loop independently from the shape control and provide the shape controller with a vertically stable plasma.

The omission of the passive structures is important only for the description of fast transients and when time constants shorter than the vessel eddy currents ones are required. The model does not show the oscillatory behaviour observed at frequencies close to the vessel eddy current time constants. The vessel mode represent the limiting factor in the choice of the response times of the various loops. The experience gained with the previous controller in terms of achievable response times is used as a guideline for the choice of the response times in the design.

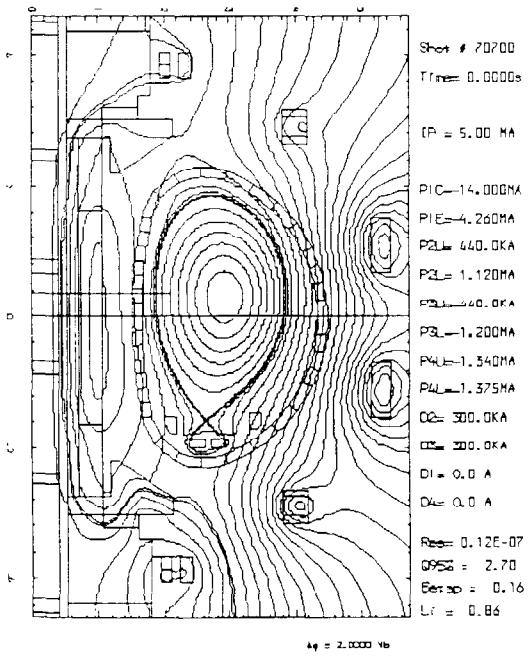

Figure 1 Plasma FAT configuration, the JET vessel and coils.

Equation (2) establishes the differential equation which describing the evolution of the PF currents including the plasma current. Matrices and arrays are indicated with bold characters. In the case of JET, ten PF currents including the plasma current I_p have to be considered. The other nine currents are (Figure 1): the primary inductor current I_M, the vertical field current I_{VF}, a radial field current used

for plasma shape purposes only I_R (not for the vertical stabilisation), the current difference in the primary inductor current I_{FX}, the shaping current which is a fixed combination of the coils P2 and P3 current (I_{SH}) and the four divertor currents ($I_{D1}, I_{D2}, I_{D3}, I_{D4}$).

The first equation can be linearised around an equilibrium position for small variations of the external currents, the plasma current and the assumed disturbances:

$$\delta \mathbf{X} = \frac{\partial \mathbf{X}}{\partial I_p}\delta I_p + \frac{\partial \mathbf{X}}{\partial \mathbf{I_C}}\delta \mathbf{I_C} + \begin{bmatrix} \frac{\partial \mathbf{X}}{\partial \beta_p} & \frac{\partial \mathbf{X}}{\partial l_i} & \frac{\partial \mathbf{X}}{\partial \psi_{iron}} \end{bmatrix} \begin{bmatrix} \delta\beta_p \\ \delta l_i \\ \delta\psi_{iron} \end{bmatrix} \tag{3}$$

A generic equilibrium variation can be written as:

$$\delta \mathbf{X} = I_P^{-1}\mathbf{B}_P \delta I_P + I_P^{-1}\mathbf{B}_C \delta \mathbf{I}_C + \mathbf{G}\begin{bmatrix} \delta\beta_p \\ \delta l_i \\ \delta\psi_{iron} \end{bmatrix} \tag{4}$$

where:

$$\mathbf{B}_P = \frac{\partial \mathbf{X}}{\partial I_P} I_P \qquad \mathbf{B}_C = \frac{\partial \mathbf{X}}{\partial \mathbf{I_C}} I_P \tag{5}$$

$\mathbf{B_P}$ and $\mathbf{B_C}$ are normalised to the equilibrium plasma current in order to get coefficients independent from the value of I_P.

$$\mathbf{G} = \begin{bmatrix} \frac{\partial \mathbf{X}}{\partial \beta_p} & \frac{\partial \mathbf{X}}{\partial l_i} & \frac{\partial \mathbf{X}}{\partial \psi_{iron}} \end{bmatrix} \tag{6}$$

$\mathbf{G}$ represents the matrix of the disturbances and will be useful for the study of the closed loop behaviour of the system. In order to simplify the model calculation the disturbance terms will be dropped in the linearisation of the second equation and added at the end.

The execution of the time derivative in (2) yields a *modified and reduced system*. The steps needed are detailed below. The (2) is written explicitly as:

$$\begin{bmatrix} \ell_P & \mathbf{M}_{PC} \\ \mathbf{M}_{CP} & \mathbf{M}_C \end{bmatrix} \begin{bmatrix} \delta\dot{I}_p \\ \delta\dot{\mathbf{I}}_C \end{bmatrix} + \begin{bmatrix} r_P & \mathbf{0} \\ \mathbf{0} & \mathbf{R}_C \end{bmatrix} \begin{bmatrix} \delta I_p \\ \delta \mathbf{I}_C \end{bmatrix} = \begin{bmatrix} 0 \\ \delta \mathbf{V}_C \end{bmatrix} \tag{7}$$

The first row highlights the plasma self inductance and the coupling between plasma and coils. The coil submatrix $\mathbf{M_C}$ does not depend on the plasma shape or the plasma current profile, while the terms of the mutual coupling between plasma and coils do.

The first step consists in extracting the plasma current equation alone.

$$\frac{d}{dt}\left(\ell_P I_P + \sum_{i=1}^{N_C} m_{PCi} I_{C_i}\right) + r_P I_P = 0 \qquad (8)$$

The execution of the time derivative yields:

$$\frac{\partial \ell_P}{\partial \mathbf{X}} \dot{\mathbf{X}} I_P + \ell_P \dot{I}_P + \sum_{i=1}^{N_C} \frac{\partial m_{PCi}}{\partial \mathbf{X}} \dot{\mathbf{X}} I_{C_i} + \mathbf{M}_{PC} \dot{\mathbf{I}}_C + r_P I_P = 0 \qquad (9)$$

Deriving the (4) against time (with $\mathbf{G} \equiv \mathbf{0}$) and substituting the result in (4) the final form of this equation is obtained:

$$\tilde{\ell}_P \, \delta \dot{I}_P + \tilde{\mathbf{M}}_{PC} \, \delta \dot{\mathbf{I}}_C + r_P I_P = 0 \qquad (10)$$

where:

$$\tilde{\ell}_P = \ell_P + \tilde{\mathbf{M}}_{PC} \mathbf{B}_P$$

$$\tilde{\mathbf{M}}_{PC} = \mathbf{M}_{PC} + \tilde{\mathbf{M}}_{PC} \mathbf{B}_C \qquad (11)$$

$$\tilde{\mathbf{M}}_{PC} = \frac{\partial \ell_P}{\partial \mathbf{X}} + \sum_{i=1}^{N_C} \frac{\partial \tilde{m}_{PCi}}{\partial \mathbf{X}}$$

The second part of the equation concerns the PF coil currents and their coupling with the plasma. The derivative in this case is:

$$\frac{\partial \mathbf{M}_{CP}}{\partial \mathbf{X}} \dot{\mathbf{X}} I_P + \mathbf{M}_{CP} \dot{I}_P + \mathbf{M}_C \dot{\mathbf{I}}_C + \mathbf{R}_C \mathbf{I}_C = \mathbf{V}_C \qquad (12)$$

where:

$$\frac{\partial \mathbf{M}_C}{\partial x_i} = \mathbf{0} \qquad i = 1, \ldots\ldots, N_G \qquad (13)$$

because the mutual inductances of the coils are not affected by plasma shape changes. Using (4) again the equation becomes:

$$\tilde{\mathbf{M}}_{CP}\,\delta\dot{\mathbf{I}}_P + \tilde{\mathbf{M}}_C\,\delta\dot{\mathbf{I}}_C + \mathbf{R}_C\mathbf{I}_C = \mathbf{V}_C \tag{14}$$

where:

$$\tilde{\mathbf{M}}_{CP} = \left(\mathbf{M}_{CP} + \frac{\partial \mathbf{M}_{CP}}{\partial \mathbf{X}}\mathbf{B}_P\right) \tag{15}$$

$$\tilde{\mathbf{M}}_C = \left(\mathbf{M}_C + \frac{\partial \mathbf{M}_{CP}}{\partial \mathbf{X}}\mathbf{B}_C\right) \tag{16}$$

The overall system can be re-written using a matrix notation as:

$$\begin{bmatrix} \ell_P & \tilde{\mathbf{M}}_{PC} \\ \tilde{\mathbf{M}}_{CP} & \tilde{\mathbf{M}}_C \end{bmatrix}\begin{bmatrix} \delta\dot{\mathbf{I}}_P \\ \delta\dot{\mathbf{I}}_C \end{bmatrix} + \begin{bmatrix} r_P & \mathbf{0} \\ \mathbf{0} & \mathbf{R}_C \end{bmatrix}\begin{bmatrix} \delta\mathbf{I}_P \\ \delta\mathbf{I}_C \end{bmatrix} = \begin{bmatrix} 0 \\ \delta\mathbf{V}_C \end{bmatrix} - \mathbf{f}\left(\beta_p, l_i, \psi_{iron}\right) \tag{17}$$

where the disturbances are:

$$\mathbf{f}\left(\psi_c, \beta_p, l_i\right) = \frac{\partial \mathbf{M}}{\partial \beta_p}\dot{\beta}_p + \frac{\partial \mathbf{M}}{\partial l_i}\dot{l}_i + \frac{\partial \mathbf{M}}{\partial \psi_c}\dot{\psi}_c \tag{18}$$

The last step consists of eliminating the plasma current from the system. The order of the system is reduced and allows for the design of the control law in the space of PF coil currents.

Since the plasma time constant is in the order of tens of seconds during the flattop phase it is possible to assume that $r_p = 0$. The (14) can be re-written as:

$$\delta\dot{\mathbf{I}}_p = -\frac{1}{\tilde{\ell}_p}\tilde{\mathbf{M}}_{PC}\delta\dot{\mathbf{I}}_C \tag{19}$$

The initial conditions are all zero, which implies that the equation can be integrated and used for the plasma current itself.

Substituting (19) in (17) and in (4) the final form of the plasma model is obtained:

$$\mathbf{M}_S\delta\dot{\mathbf{I}}_C + \mathbf{R}_C\delta\mathbf{I}_C = \mathbf{V}_C - \mathbf{f}\left(\beta_p, l_i, \psi_{iron}\right)$$

$$\delta \mathbf{X} = \mathrm{I}_{\mathrm{P}}^{-1} \mathbf{B}_{\mathrm{S}} \delta \mathbf{I}_{\mathrm{C}} + \mathbf{G} \begin{bmatrix} \delta \beta_{\mathrm{p}} \\ \delta \mathrm{l}_{\mathrm{i}} \\ \delta \psi_{\mathrm{iron}} \end{bmatrix} \tag{20}$$

$$\delta \dot{\mathrm{I}}_{\mathrm{P}} = -\frac{1}{\tilde{\ell}_{\mathrm{P}}} \tilde{\mathbf{M}}_{\mathrm{PC}} \delta \dot{\mathbf{I}}_{\mathrm{C}}$$

where:

$$\mathbf{M}_{\mathrm{S}} = \left(\tilde{\mathbf{M}}_{\mathrm{C}} - \frac{1}{\tilde{\ell}_{\mathrm{p}}} \tilde{\mathbf{M}}_{\mathrm{PC}} \tilde{\mathbf{M}}_{\mathrm{CP}} \right) \tag{21}$$

$$\mathbf{B}_{\mathrm{S}} = \left(\mathbf{B}_{\mathrm{C}} - \frac{1}{\tilde{\ell}_{\mathrm{P}}} \mathbf{B}_{\mathrm{P}} \tilde{\mathbf{M}}_{\mathrm{PC}} \right) \tag{22}$$

In its final form, the system is *modified* by the presence of the plasma equilibrium equation and *reduced* by the linear dependence of the plasma current variation from the other circuit currents.

The open loop model is not complete unless some hypothesis are drawn on the power supplies which drive the coil voltages.

The JET power supplies driven by the shape control are conventional 50 Hz 12 pulses AC-DC thyristor bridges. Their small voltage signal response time is less than 2ms. These amplifiers are modelled as pure gains with one exception represented by complex of the PF generator-converter which drives the Ohmic Heating (OH) circuit in JET [3.]. This is a slow system with an equivalent first order time constant of 250ms or more in the voltage response. This violates the hypothesis on the fast response time of the actuators. Moreover, contrary to the previous design [8.] for the plasma current control the generator is considered to behave like a voltage source.

Two different approaches can be considered for the inclusion of the generator in the decoupling scheme. The first one [7.], [6.] is the classical technique of series connecting two state space described systems. This method has the marked disadvantage of increasing unnecessarily the order of the overall system without solving the problem of the varying characteristics of the generator

[8.]. The second method consists of placing the inverse transfer function of the generator directly in the loop using a direct pole cancellation approach. This method is preferred for its simplicity and the generator compensation was included in the system simulations used to validate the design.

3. Controller Design

The controller design consists of two steps. The first defines the controller structure and its suitability for the flattop phase. The second verifies that it is adequate to cover all the various phases of the pulse.

This phase of the design will also cover the constraints on the possible choices for the gaps to be controlled and some numerical considerations on the system linearity.

The controller designed here is a *multivariable decoupling controller*. This means that we want that all the coils in the system change their currents in order to achieve a particular gap demand, but no other gap is allowed to vary. Moreover we want to be able to choose the time response of each loop independently. We also require static errors in the gaps less than 1cm and static errors in the coil currents less the 150A.

The controller a matrix **K** is defined as the product of two matrices **E** and **C**:

$$\mathbf{K} = \mathbf{E}\,\mathbf{C} \tag{23}$$

C is a diagonal matrix whose elements are the desired eigenvalues of each loop and **E** is the decoupling matrix, chosen to diagonalise the closed loop system.

In case on current control for all the circuits the choice of the control matrix is trivial. The matrix:

$$\mathbf{E} = \mathbf{M}_s \tag{24}$$

Solves the decoupling problem. The closed loop equation becomes:

$$\mathbf{M}_s \dot{\mathbf{I}}_C + \mathbf{R}\mathbf{I}_C = -\mathbf{E}\mathbf{C}\left(\mathbf{I}_C - \mathbf{I}_{ref}\right) \tag{25}$$

Static errors are present due to the finite values of the resistances in the matrix **R**. The JET coils time constants are very long (seconds) with respect to the desired control time constants (10-100ms). Therefore the resistive voltage is a minor fraction of the control effort in most circumstances.

If coil currents are fed back through a matrix $\mathbf{D} \cong \mathbf{R}$ using a positive feedback loop, the coils will appear as superconductive (*resistive compensation)*. A small fraction of positive feedback is applied when compared to the decoupling action, given the coils time constants. The fine tuning of **D** is carried out experimentally.

$$\mathbf{M}_s \dot{\mathbf{I}}_C + \mathbf{R}\mathbf{I}_C = -\mathbf{E}\mathbf{C}(\mathbf{I}_C - \mathbf{I}_{ref}) + \mathbf{D}\mathbf{I}_C \qquad (26)$$

The system eigenvalues are the ones of the matrix $\mathbf{M}_s^{-1}\mathbf{E}\mathbf{C}$ and therefore are the eigenvalues of **C** in case of perfect matching between the plant and the controller matrices

A linear transformation **T** between the set of quantities **Y** to be controlled and the PF currents is needed to design the gap control. The array **Y** consists of the plasma current, a set of gaps and a subset of PF currents to be directly controlled such as to get always nine degrees of freedom to control:

$$\delta\mathbf{Y} = \delta\begin{bmatrix} \mathbf{I}_p \\ \mathbf{X}_s \\ \mathbf{I}_s \end{bmatrix} = \begin{bmatrix} -\frac{1}{\tilde{\ell}_p}\tilde{\mathbf{M}}_{PCi} \\ \mathbf{I}_p^{-1}\mathbf{B}_s \text{rows} \\ \text{unity matrix rows} \end{bmatrix} \delta\mathbf{I}_C = \mathbf{T}\delta\mathbf{I}_C \qquad (27)$$

It can be noted that from the mathematical point of view the plasma current behaves like a gap in the control scheme, if the **B** matrix rows are substituted by the $\tilde{\mathbf{M}}_{PCi}$ array.

Ignoring the PF coils resistance and the disturbance terms, the generic form of the controller **K** is:

$$\mathbf{K} = \mathbf{M}_s \mathbf{T}^{-1} \mathbf{C} = \mathbf{E}\mathbf{C} \qquad (28)$$

A controller of this form diagonalises the overall closed loop system and imposes the closed loop eigenvalues of the matrix **C**. The condition to safeguard is that the matrix **T** remains far from being singular. This condition is achieved by a judicious choice of the gap combinations allowed in simultaneously in the control. Attempts to control gaps which result in having rows of **B** almost proportional are therefore dangerous.

Having discussed above the little efficiency of the shaping current I_{SH} for the gap control it is evident that this current is always directly controlled. On the contrary the divertor coils 1 and 4 are always left in current control not to get near singular situations in the matrix **T**. This limits the maximum number of gaps which can be controlled at the same time to five plus the plasma current.

The voltage to be applied to the PF coils is therefore:

$$\mathbf{V}_C = \mathbf{R}\,\mathbf{I}_C + \mathbf{K}\left(\mathbf{Y}_{ref} - \mathbf{Y}\right) \qquad (29)$$

where the resistive term is applied as a positive feedback term to suppress the effect of the finite coil resistance.

The algorithm adopted allocates all the closed loop eigenvalues and allows complete freedom in the choice of the time constants of each loop through the matrix **C**. However the method does not use weight matrices like in LQR algorithms that allow for a limited voltage range or that restricts the action of a power supply on a certain gap. For a given gap (or current) y_i all nine power supplies respond with the time constant τ_i assigned to that loop. If this fact is combined with the observation that the decoupling matrix is never going to match accurately the actual plant parameters it becomes obvious that the **K** given by the (7) can be altered by deleting terms which link coils with limited voltage capabilities to gaps which demand a fast response time. In other words, the circuits which produce a significant fraction of radial field compared with vertical field can be asked to work hard by the selection of the time responses in the matrix **C** on gaps for which they are not efficient. This fact can be corrected a posteriori by deleting some crucial terms in the matrix **K**.

A typical example of this arrangement is provided by the interaction between the radial field current I_R the outer gap, mostly dependent from the vertical field. The imbalance circuit comprises 122 turns and has a voltage capability at present of ±1500V. The radial field is highly inefficient for the control of the outer gap which has a fast response time (20ms). Therefore the term in the matrix **K** relating the action of imbalance on the outer gap is suppressed. Similarly other coefficients of the final matrix are altered by an element by element multiplication of the elements of **K** by the ones of a matrix **H** (zeros or ones) to get a modified **K** for the gap control:

$$\tilde{k}(i,j) = h(i,j) * k(i,j) \qquad (30)$$

The heat load on to the JET Mark-1 divertor needs spreading for high performance pulses. This is achieved by increasing the effective scrape-off area of the plasma by sweeping radially the separatrix at 4Hz using either a sinusoidal or a triangular reference. In order to achieve a triangular sweeping (12Hz for the third harmonic or above) time constants in the order of 10-20ms are assigned to the control of the X-point or the Strike point. Moreover the radial position control in front of the RF antennae needs to be fast in order to maintain a good coupling when heating is applied.

In the attempt to limit the choice of higher gains and to extend the operating range of the system the control scheme can include a feedforward action. Since all the power amplifiers are voltage sources the feedforward has to be a voltage. However, for convenience of use, current feedforwards are preferred. After derivation and multiplication by the plant inductance matrix the correct voltages are applied (Figure 2).

No study has been carried out to check that the vessel currents do not affect the desired time responses. No detailed study using the *z-transformation* or other discrete time design method has been used since the sampling frequency of the controller has been fixed to 500Hz which gives rise

to a quasi analogue realisation of the design above. The experimental evidence shows that the simplifications used in the design were justified.

The coefficients of the matrix **B** were calculated for a wide range of plasma configurations and levels of plasma current. The aim of the calculation was to measure the robustness of the controller to plant variations. The result is shown in figure 3a and 3b. The figures show the position of the closed loop eigenvalues for a nominal case and the movement of the eigenvalues when the plant is described by matrices **B** different from the one used in the controller calculation.

Parametric changes in the plant description result in differences between the design eigenvalues and the real eigenvalues in the closed loop system. It can be seen that the controller is quite robust, in the sense that the eigenvalue position do not change substantially and do not significantly decrease the overall stability margin. This is due to the arrangement of the JET coils in circuits which are mostly coupled to one of the gaps chosen. This characteristic of the system, together with a careful choice of the gaps location, allows for rather large variations in the plant coefficients without influencing significantly the closed loop eigenvalues.

4. Numerical Considerations

The calculation of the various matrices and arrays described in the previous section has been carried out using the PROTEUS code [4., 5.]. PROTEUS is a 2D finite element free boundary equilibrium code. The calculations of the matrices derived from equations (1) and (2) is carried out using the *direct* implementation available at JET.

The code finds the solution of the Grad-Shafranov equation given the PF coils currents, the plasma current profile as a function of the poloidal flux, and the value of the plasma current. The iron core of the JET machine is described by means of a permeability curve.

The plasma current profile is described by a family of functions as described below:

$$j(\psi)=\left(\frac{R}{R_0}\delta+\frac{R_0}{R}(1-\delta)\right)(1-\bar{\psi})^{\alpha} \tag{31}$$

where $\bar{\psi}$ is the poloidal flux normalised to one on the plasma axis:

$$\bar{\psi}=\frac{\psi \quad -\psi_{boundary}}{\psi_{axis}-\psi_{boundary}} \tag{32}$$

it can be seen that:

$$\begin{aligned}\delta &\cong \beta_p \\ l_i &\cong \alpha\end{aligned} \tag{33}$$

The direct implementation is appropriate to calculate the **B** matrix. A variation to each of the circuit currents is applied to a given plasma equilibrium while keeping all the other currents constant. The procedure is quite tedious since its needs to be repeated for all the equilibria to be studied. In particular, shape changes based on the variation of l_i and β_p were considered to check the effects of additional heating and current rise to the model.

The procedure was applied to a database of configurations at different levels of plasma current, applying positive and negative excursion of each current to test the limit of the linear range. This is particularly important since large non linearities could pose a problem in the feedback loop if not treated properly.

The extensive calculations carried out demonstrated that the variations in the closed loop eigenvalues are not large and therefore a single matrix **B** in the controller calculation is sufficient to handle a whole pulse and a range of configurations.

The effect of the *Shaping Circuit* is irrelevant to most of the gaps. This is due to the highly inflexible properties of this circuit once the turns ratio of the P2 and P3 (Figure 1) coils have been fixed. A better definition of the shape of the plasma top could be achieved by splitting the circuit and controlling individually the top P2 and P3 coils.

The present arrangement leads to the selection of a gap in the machine top which is not in the middle of the chamber. Either the distance between the inner saddle coil or the distance with the outer saddle coil and the plasma can be chosen. The inner one is the most likely interaction point between the plasma and the walls and therefore is chosen. The Top gap referred to is defined as above.

The PROTEUS code is also used for the calculation of the inductance matrix **M** and its derivatives with respect to the various gaps considered. The limitations in the calculations are imposed in this case by the nature of PROTEUS as a direct code.

The mutual inductances between the various coils can be evaluated by:

$$m_{ij} = \left.\frac{\partial \psi_i}{\partial I_j}\right|_{I_i = \text{constant for } i \neq j} \qquad (34)$$

where ψ_i is the flux linked to the coil i by the variation of the j-th current.

The calculation expressed by the (4) implies that the plasma boundary should be frozen during the current variation δI. This is not possible because PROTEUS is a direct free-boundary code.

It would be more convenient to consider an approach like [10.] which gives directly the modified matrix. PROTEUS imposes the total plasma current and therefore the flux conservation law is violated whenever a net flux is injected into the plasma.

The calculation is of the inductance matrix is carried out using four filaments to replace the plasma current, positioned such as to reproduce the shape of the equilibrium with good accuracy. The derivatives of the mutual inductances with respect to a radial and vertical movements of the filaments instead of the actual gaps are considered because of computational difficulties in executing the derivatives with respect to the gaps. This is quite justified because the *matrix modification* due to the plasma presence (15, 16) is small already for the terms which are purely radial or vertical.

The results obtained for the inductances and their derivatives are consistent with the ones calculated with the electromagnetic code JACOB [11.] which uses a distributed current J(R,Z) to describe the plasma and is calculates the inductances and their derivatives through the application of analytical formulas.

5. Real Time Plasma Boundary Measurement

The plasma boundary is measured in real time at the same frequency of the shape controller. The Xloc algorithm [9.] is used for this purpose. The shape control system receives 91 magnetic signals from the new JET magnetic diagnostic. The signals are either normal poloidal field measurement from saddle loops mounted outside the vacuum vessel or tangential field measurement using Mirnov coils. In addition the new probes mounted for the divertor diagnosis on the target are received. They also consists of a set of saddle loops measurements and tangential and normal field measurement on the target.

The Xloc algorithm can be described as a two-dimensional Taylor series expansion around some centre points joint together by a minimisation process. The JET vacuum vessel is divided into five regions tied together to yield a coherent boundary reconstruction. The calculation of twelve plasma-wall distances plus the X-point location takes about 1ms calculation time on one TMS 320C40 processor.

The plasma-wall distances measurement involves the following steps:

1. A precalculated matrix which depends only on the physical location of the magnetic probes is multiplied by the array of the measurements to give the set of the XLOC Taylor coefficients which define the flux function everywhere outside the plasma.

2. The minimum (or maximum) flux value on the vessel wall is calculated on a predetermined set of 100 points. The direction of the plasma current in a right hand sided reference system determines if a maximum or a minimum of the flux has to be searched for.
3. A field null is searched to find whether an X-point is present.
4. The flux at the field null and the minimum (maximum) wall flux are compared to determine if the configuration is limiter or X-point.
5. The plasma-wall distances are calculated along predetermined lines at fixed wall locations.

This algorithm is quite robust and measures the plasma-wall distances at all the points that are away from the extrapolation region junctions with errors in the centimeters range. Some general remarks on fast plasma boundary measurement methods for a control system are added.

The plasma boundary measurement works reliably when the plasma configuration is not dominated by stray fields. This implies that the breakdown phase, or in general transitions between no-plasma plasma situations are not handled correctly. In general a minimum level of plasma current (in the JET application this is around 500kA) can be used as a guideline for a good reconstruction.

One way of using the code would be to run the χ^2 check on the reconstructed signals to define when the code results are reliable. However more empirical approaches, like setting a value of the plasma current below which the code results are discarded can be used.

The advantage of the χ^2 check is that improves the reliability of the overall reconstruction. The failure of a single signal can be picked up in real time and acted upon. At present χ^2 checks are not implemented in the JET Shape Controller, although its design includes the possibility of detecting such failures and use a *termination scenario* based on the acquisition of a reduced set of magnetic signals from an analogue source.

6. Experimental Results

The shape controller has been commissioned and tested during the JET 1994 campaign and is used routinely for the JET operation. Initial results were reported in [13]. Here a more comprehensive set of results is provided.

Figure 4 shows pulse 30482. After t = 12s the control of the plasma radial position is done through the outer gap. The reference waveform is joined to the measured value at the time the control mode is changed. Before t = 12s the plasma radial position was controlled by means of the flux error, similarly to [3]. Around t = 14s and t = 16s the reference waveform asks for plasma radial movements of 2cm. The effect of these requests can be observed in the inner gap which mirrors the behaviour of the outer gap and in the quantities which depend mostly from the vertical field, like the X-point radius and the top gap. All the other currents are kept in direct current control, apart from the magnetising current which controls the plasma current.

Figure 5a shows the simultaneous control of the inner and the outer gaps in pulse 30617. Again, at t = 12s the gaps are directly controlled. First it can be observed that the flux control keeps the plasma generally in position radially, but gives several centimetres error between the reference and the actual value for an X-point configuration, where the reference point for the flux is uncertain. The control of the inner gap shown in figure 5a shows a static error of order 1-1.5cm which is not dealt with by the resistive compensation. In order to avoid the steady state error, an integrator with a 1s time constant was inserted in the loop with the result shown in figure 5b.

Figure 6 shows the control of the complete configuration as per the design. The gaps directly controlled in this case are the outer gap, the inner gap, the top gap, the X-point radial position and the X-point vertical position. At t = 14s the control mode of the system is switched from current control to gap control. Triangular sweeping of the X-point radial position is applied at 4Hz. Ramps and steps in the reference waveforms for the top gap and for the X-point height are applied to check

the decoupling properties. of the algorithm. Transients in the outer gap can be seen at the times when a step is requested to the X-point height. This effect is due to the non perfect decoupling action at very high frequency because of the omission of the vessel currents. This effect is considered acceptable for the performance. The effect of the radial X-point sweeping can be observed on the response of the inner gap. The inner gap modulation is due to the slow time response used in this control (100ms) compared with the one used for the X-point radius (12ms). If the movement was counteracted by choosing a faster response time the PFX amplifier, which controls the current difference in the magnetising circuit, would be driven to full voltage saturation requiring large power swings to and from the electricity network (80MW).

A comparison between figures 6 and 4 shows the ability of the system to perform the decoupling action between the various controlled quantities.

Figure 7 shows the same experiment as figure 6 with the application of additional heating. The two configurations shown are one in Ohmic regime and the other in H-mode. The poloidal beta changes from 0.1 in for the Ohmic plasma to 0.7 for the heated one. The configuration is well controlled at the control points. It can be seen that on the top outer part of the machine, where no gap control is used there is instead a noticeable difference in the position of the magnetic separatrix. A split of the shaping circuit would allow the control of the outside position.

Figure 8 shows a fundamental feature of the control system. If a current in an amplifier saturates without the knowledge of the control system the result is the loss of stability, because a degree of freedom is lost. In pulse 30269 this feature is illustrated by the control of the top gap and the imbalance current I_R which constitutes the principal actuator for it. The controller is asked to increase the top gap after 15s. The I_R limit is fixed at -5kA (one third of the normal range) and is hit in the experiment. The top gap control is abandoned and the limit is tracked until the plasma current decrease and the top gap demand bring it back into range.

The gap control was initially designed only for X-point configurations, where the plasma behaves more like a rigid body (see figure 4). The precision in the control obtained has created the interest to extend its performance for limiter plasmas. The main problem encountered in trying to extend the performance is the impossibility of certain types of control when the plasma rests on a wall. The problem of the radial position control is particularly sensitive. The gap control is non-linear around the zero values of the gaps. If the outer gap is requested to be zero the controller is not capable of calculating the correct vertical field voltage needed to avoid that the plasma shrinks to the outside of the machine and collapses when the $q = 2$ limit is overtaken.

The problem is solved in JET by asking the vertical field coils to control the inner plasma wall distance when plasma is required to lie on the outer wall and abandon the control of the inner gap which would make the system overdetermined. The change in control mode is achieved by changing rows in the transformation matrix **T** in (27).

The result of this choice are illustrated in figure 9. The outer and the inner gap references ask for an outside plasma shift. When the plasma is brought to the outer wall the control of the inner gap is abandoned and the current of PFX is tracked at the value measured at the moment of contact. The control is switched back when the plasma is moved outside again.

7. Conclusions

This paper provides the basis of the theoretical design and the discussion of the experimental results of the JET Plasma Shape and Current Control system. A method for plasma shape control has been implemented in closed loop for the first time on JET with good results, allowing the control of critical plasma-wall distances or key shape parameters like the strike point position.

The method illustrated results in a simple control algorithm experimentally proven to be versatile and robust enough to cope with different plasma configurations and the operational requirements of

JET. The system in its present implementation provides the basis for the experimentation of other controllers to check the suitability of more sophisticated control methods indicated at present for ITER.

Acknowledgements

The authors wish to thank Drs. P. Noll and E. Bertolini for their help and guidance during the design phase of the control system, Drs. A. Tanga and D. Campbell for their active help and enthusiasm for commissioning the system, Drs. D. O'Brien and J.J. Ellis for the help provided with the Xloc algortihm.

References

[1.] M. Garribba, R. Litunovsky, P. Noll, S. Puppin, The New Control Scheme for the JET Plasma Position and Current Control Scheme, XV SOFE, Hyannis, Massachusetts, 11-15 October 1993.
[2.] J. Last, P. Barabaschi, E. Bertolini, M. Garribba, M. Huguet, P. Noll, P. H. Rebut, C. Sborchia, The JET divertor magnetic configuration and coil design, Fusion Technology Proceedings of XVI SOFT, London 1990, pp. 1614-1618.
[3.] E. Bertolini, P. L. Mondino, P. Noll The JET Magnet Power Supplies and Plasma Control Systems, Fusion Technology, January 1987, Vol 11, Number 1, pp.71-119
[4.] R. Albanese, J. Blum, O. de Barbieri, Numerical Studies of the Next European Torus via PROTEUS Code, Proc. of XII Conference on Numerical Simulation of Plasmas, S. Francisco 1987.
[5.] R. Albanese, Evoluzione Temporale di un Plasma Confinato Magneticamente, Phd Thesis, Naples University, 1986
[6.] F. Franklin, G. Powell, M. Workman, Digital Control of Dynamic Systems, Addison-Wesley1990, pp. 238-322, pp. 430-441.
[7.] G. Marchesini, E. Fornasini, Appunti di Teoria dei Sistemi, Progetto Padova, 1985.
[8.] P. Silvestrin, Digital Control of the Plasma Current in JET, Phd Thesis, Padova University, 1985.
[9.] D. O'Brien, J. J. Ellis J. Lingertat, Local Expansion Method for Fast Boundary Identification at JET, Nuclear Fusion 33, 467 (1993).
[10.] R. Albanese, E. Coccorese, G. Rubinacci, Plasma Modelling for the control of Vertical Instabilities in Tokamaks, Nuclear Fusion, Vol. 29, No. 6, pp. 1013-1023, 1989.
[11.] S. Bobbio, E. Bertolini, M. Garribba, G. Miano, P. Noll, E. Senatore, An Analytic Procedure for Currents and Forces Calculation in JET, Proc. of XVI SOFT, London, 1990
[12.] Reference on the design of the new magnetic diagnostic (coil positioning)
[13.] M. Garribba, et. al., First Operational Experience with the New Plasma Position and Current Control System of JET, Proc. of XVIII SOFT, Karlsrhue 1994.
[14.] M.L. Walker, D. A. Humphreys, A. Nerem, Plasma Response Modelling for Multivariable Tokamak Control Design, GA Report GA-A21473.

[15.] D. A. Humphreys, I. H. Hutchinson, Axissymmetric Control Design in Tokamaks using Perturbed Equilibrium Plasma Response Modelling, Fusion Technology, Vol. 23, pagg 167-184, 1993.

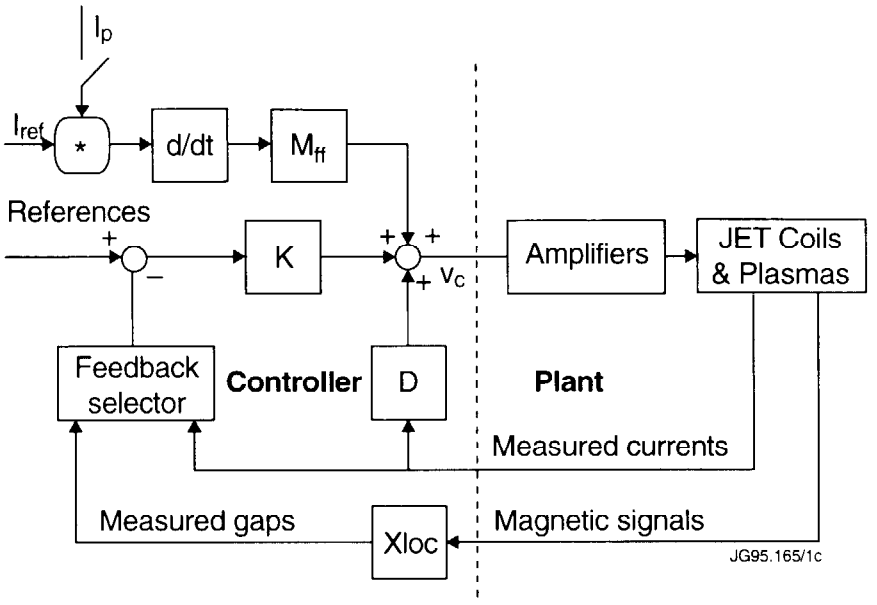

Fig.2: Shape Control Block Diagram.

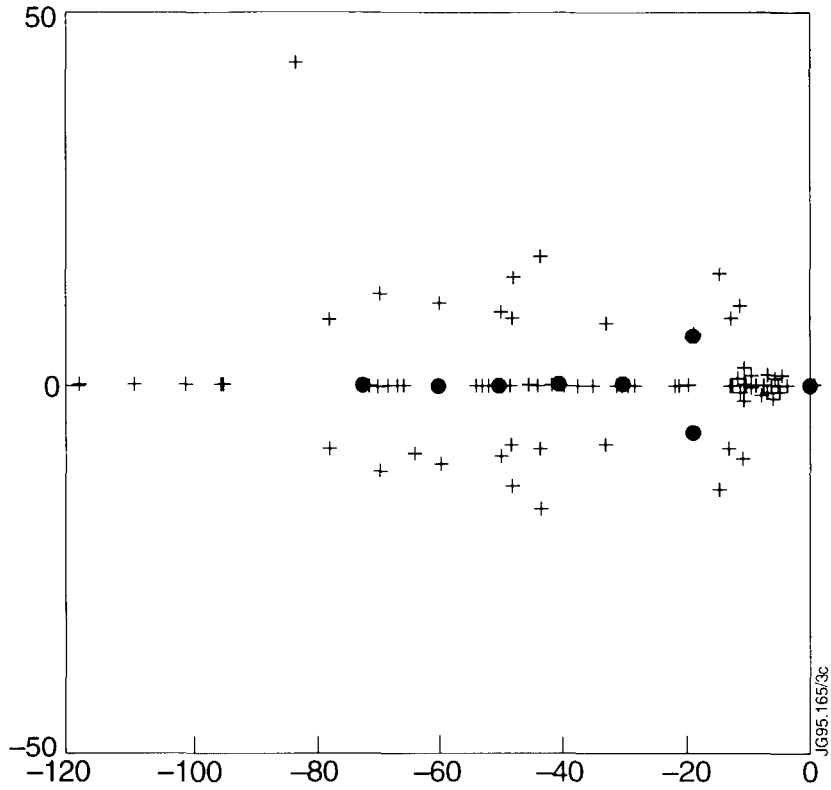

Fig.3a: Eigenvalue movement in the phase plane for different B matrices used in the controller calculation and in the plant model. Circles indicate the original eigenvalue position and crosses their relative movements.

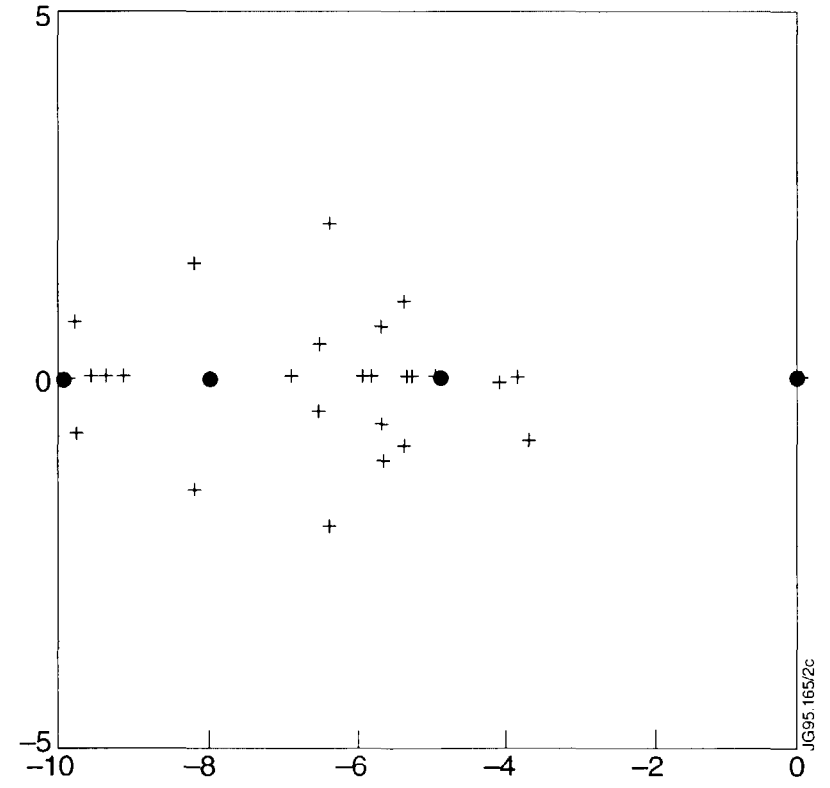

Fig.3b: Zoom on low frequency part of eigenvalue position.

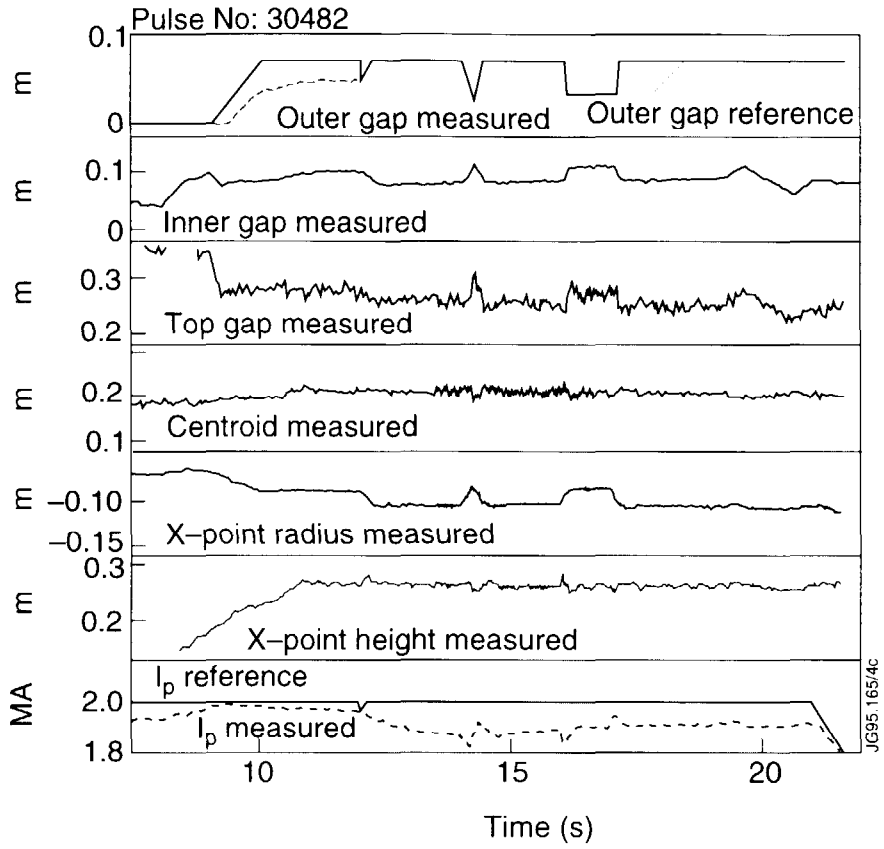

Fig.4: Outer Gap Control Only. From t=12s the Control of the outer gap is switched on changing control mode from the flux extrapolation. Note the response of the other gaps to the reference in the outer gap.

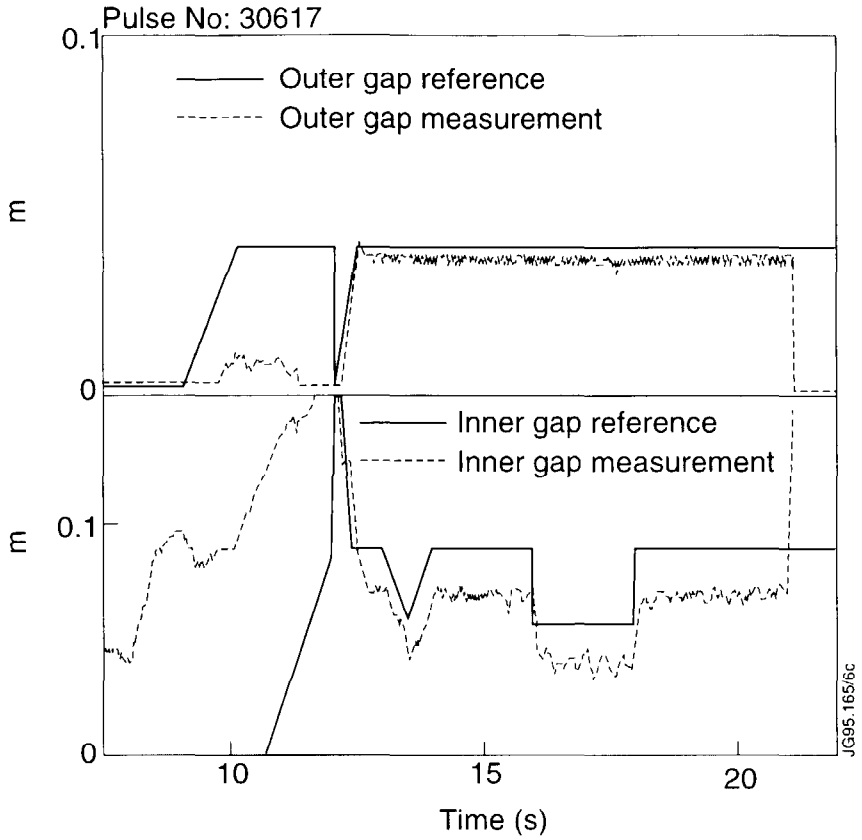

Fig.5a: Combined control of Outer and Inner Gap from t=12s. Note the static error in the Inner Gap control.

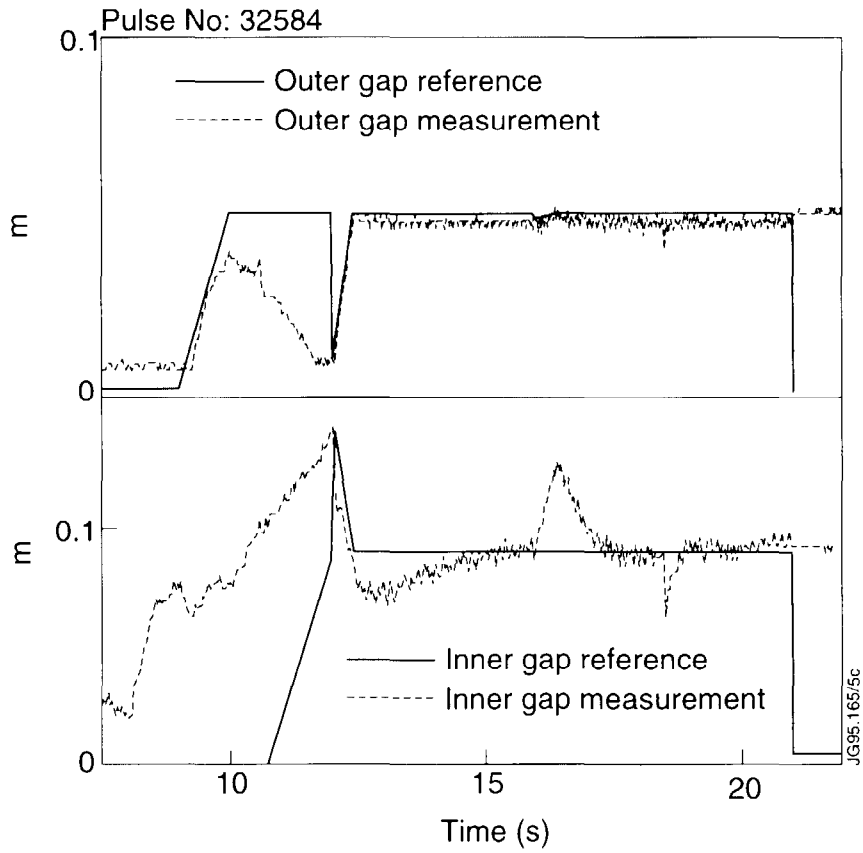

Fig.5b: Same situation after introducing an integral term on the control of the Inner Gap only.

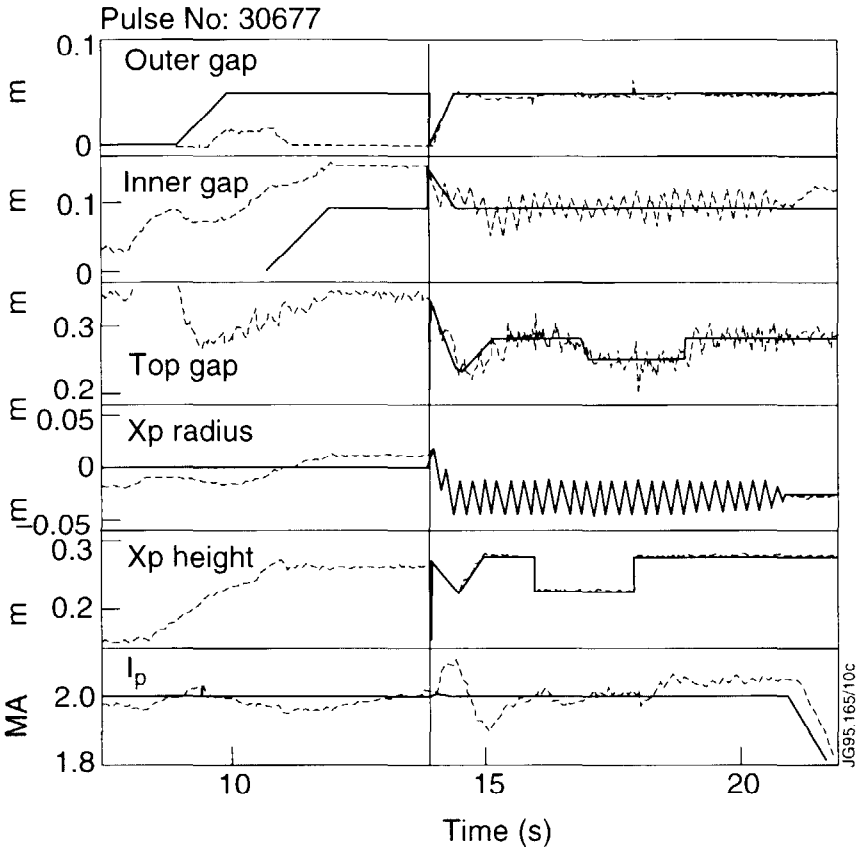

Fig.6: Control of the configuration with 4Hz sweeping. Note the effect of the radial sweeping of the X-point on the value of the Inner Gap. Solid lines show the reference waveforms for the gaps, while the dashed lines show the measured values.

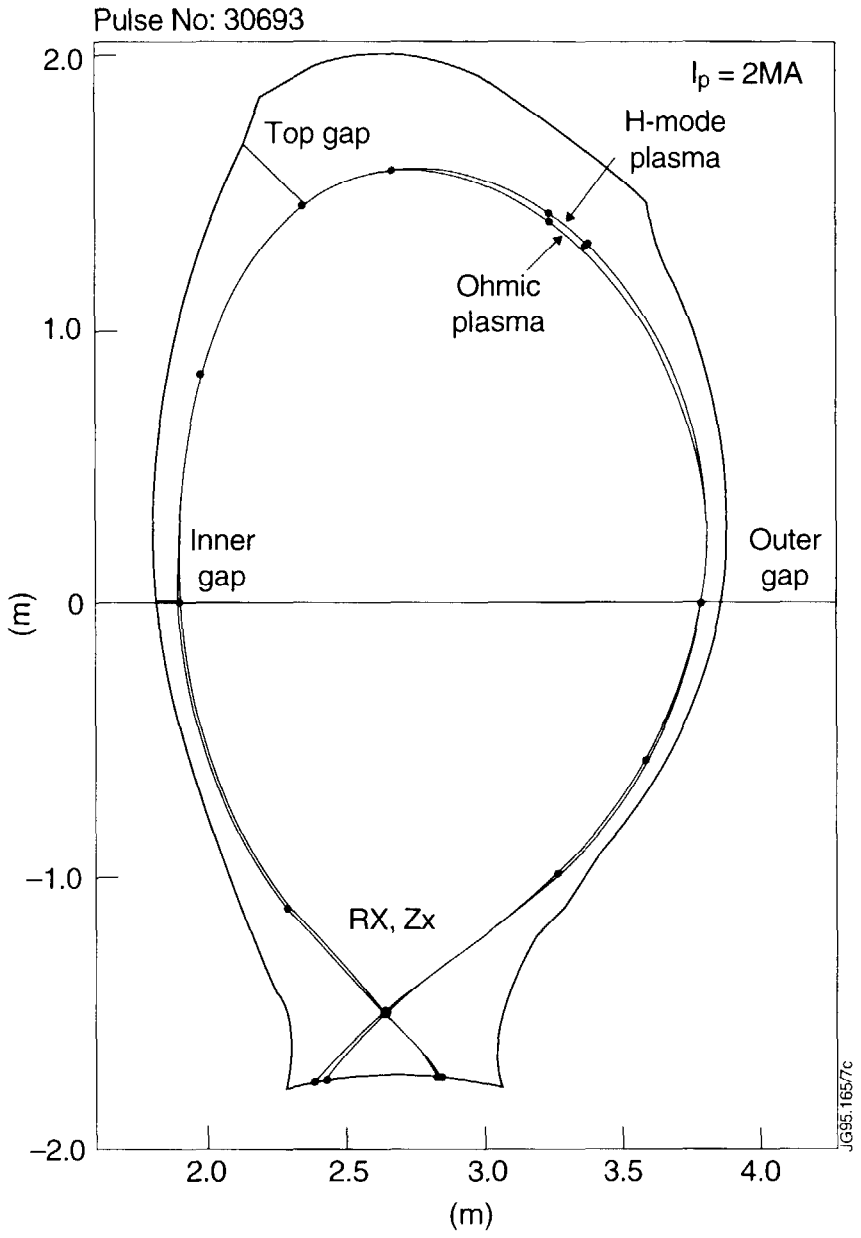

Fig.7: Control of the configuration. Location of the control points and effect of increased β_p from 0.16 to 0.5 after application of 10MW of NBI Power.

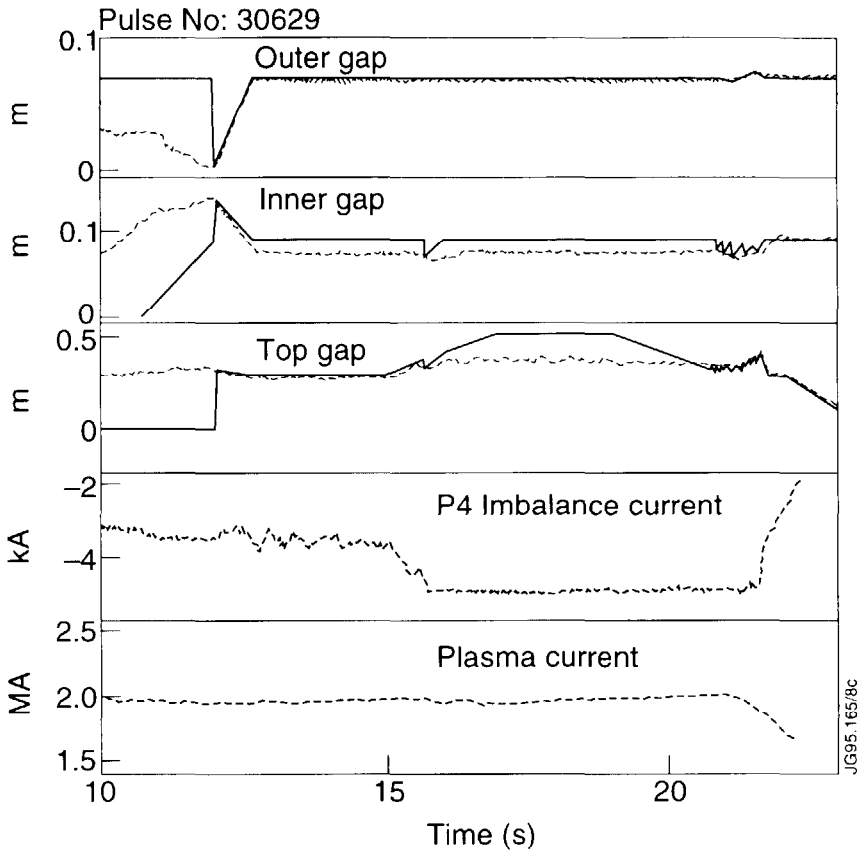

Fig.8: Effect of Current Saturation of one circuit on the controller behaviour. For the gaps solid lines show the reference waveforms, while dashed lines show the measured values.

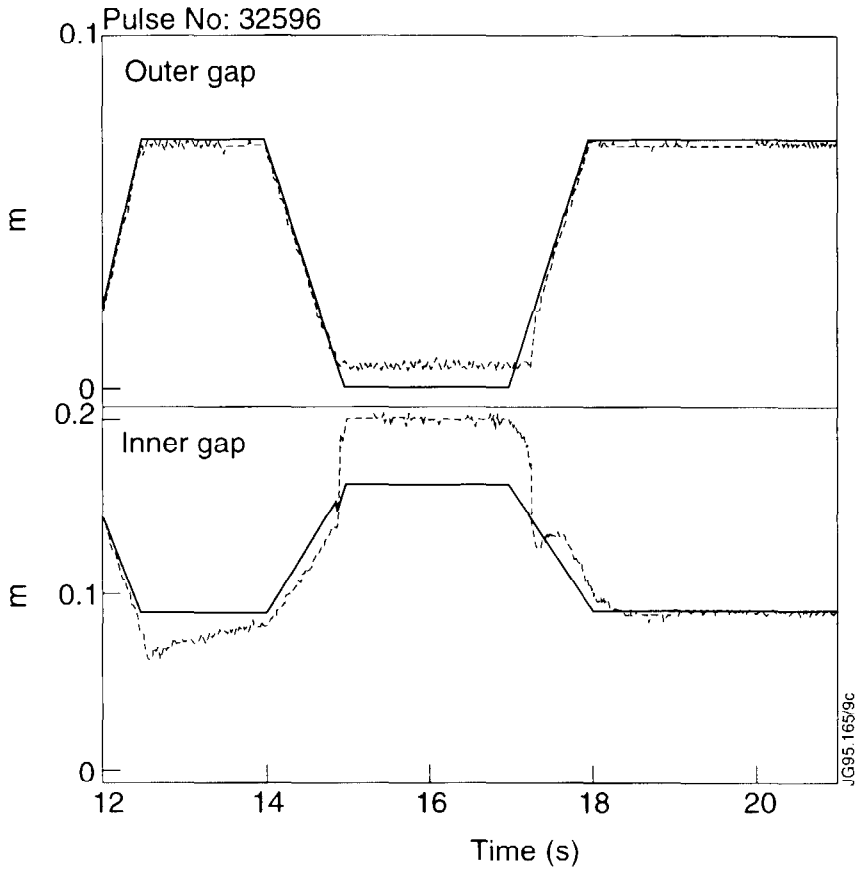

Fig.9: Control of the radial position through the Inner and Outer Gaps when the plasma leans on the outer limiter. Solid lines show the reference waveforms, while the dashed lines show the measured values.